14 Challenges from Experiment

L. Hao Tjeng
Max Planck Institute for Chemical Physics of Solids
Dresden

Contents

1 Introduction **2**
1.1 Strongly correlated materials 2
1.2 Electronic structure and synchrotron based spectroscopies 2
1.3 Challenges for theory 3

2 Spin-state transition in $LaCoO_3$ **4**
2.1 Introduction 4
2.2 Experimental 4
2.3 Results: XAS 5
2.4 Analysis 5
2.5 Results: MCD 7
2.6 Discussion 9

3 Electronic structure of NiO **9**
3.1 Introduction 9
3.2 Experimental 11
3.3 Results 12
3.4 Analysis 13
3.5 Non-local screening 15
3.6 Multi-site analysis 15
3.7 Conclusion 16

E. Pavarini, E. Koch, Dieter Vollhardt, and Alexander Lichtenstein
The LDA+DMFT approach to strongly correlated materials
Modeling and Simulation Vol. 1
Forschungszentrum Jülich, 2011, ISBN 978-3-89336-734-4
http://www.cond-mat.de/events/correl11

1 Introduction

1.1 Strongly correlated materials

One of the most intriguing aspects of transition-metal and rare-earth materials is the wide variety and richness of their physical properties. These are often quite spectacular and include phenomena such as metal-insulator transitions (MIT), colossal magneto-resistance (CMR) behavior, and superconductivity [1, 2]. It is well accepted by now that the interplay between electron correlation and band formation effects is somehow responsible for these unexpected and novel phenomena. Although conceptually clean and beautiful, theoretical simplifications in terms of, for instance, a Heisenberg model or a single band Hubbard model turn out to be inadequate [3–5]. It now becomes more and more clear that a full identification of the relevant charge, orbital and spin degrees of freedom of the metal ions involved is needed to understand the intricate balance between band formation and electron-correlation effects. An important example is the manganates [6], where orbital ordering and charge distribution [7, 8] of the Mn ions play an important role for its CMR behavior. For the newly synthesized layered cobaltates, it is the spin-state transitions that are thought to govern the CMR and MIT phenomena [9, 10]. Another example is V_2O_3 [11–13], for which it has been discovered that the orbital occupations across the various MITs change dramatically, leading to a switch of the nearest-neighbor spin-spin correlations so that in turn the effective band widths are strongly modified.
An important characteristic determining the charge, orbital and spin degrees of freedom is the presence of the so-called atomic-like multiplet interactions on the transition-metal and rare-earth ions [14, 15]. The ground state and near ground state properties could depend very much on the intricate details of these local Coulomb and exchange interactions, and how they play out in the presence of crystal or ligand fields as well as band formation. It is not trivial to describe these multiplet effects using ab-initio mean-field theories. LDA+U type of approaches, for example, utilize occupation number operators of the type $U_{ij}d_i^\dagger d_i d_j^\dagger d_j$, but these do not capture the spin and orbital flip processes contained in the $U_{ijkl}d_i^\dagger d_j d_k^\dagger d_l$ terms of the full Hamiltonian [16], leading to major errors in the total energy level diagram for both the ground state problem as well as for the excited states. In this respect an approach based on the LDA+DMFT is perhaps more promising and hopefully its implementation can be made in the very near future. It is also not trivial for real materials to determine experimentally their energy levels associated with the multiplet interactions. One often needs synchrotron based spectroscopies in order to have sufficient dynamic range in energy to map out the excitations as well as to have well defined matrix elements to quantitatively analyze the spectra.

1.2 Electronic structure and synchrotron based spectroscopies

Electron spectroscopies are powerful tools to unravel the basic electronic structure of materials. Use can be made of the extremely large dynamic range in energy that these forms of spectroscopies can cover. By studying excitation spectra in the energy range from several eV up to several hundreds of eV, one can obtain direct information about the 'bare' electrons, e.g. the

charge, spin, and orbital state of the ions that make up the correlated material. By measuring the excitation spectra in the vincinity of the chemical potential with ultra-high resolution, one can find directly the momentum dependent behavior of the 'dressed' electrons, i.e., quasi particles. In the case of photoemission or inverse photoemission, we should stress that it is not the excitation energy that determines whether the measurement probes the high or low energy scale physics. Instead, it is the resolution with which the measurement is carried out, since this determines the quality of the observed features, and thus of the measured low energy scale phenomena if the measurement is focussed on the region near the chemical potential.

There are several forms of electron spectroscopies, and which one to apply depends very much on the material and the problem that needs to be solved. While photoemission and inverse photoemission are well established techniques [17], the use of synchrotron radiation based high energy spectroscopies such as linearly and circularly polarized soft-X-ray absorption spectroscopy is relatively new [18–20,22,21]. This type of spectroscopy has been developed into full maturity only in the last 15 years, both in terms of instrumentation as well as in terms of a quantitative theoretical analysis of the spectra, which are often dominated by multiplet structures. These spectra are not only element specific, but above all, their multiplet structures are extremely sensitive to the charge, spin and orbital state of the ion due to the very effective dipole selection rules associated with the K ($1s \rightarrow 2p$), $L_{2,3}$ ($2p \rightarrow 3d$), and $M_{4,5}$ ($3d \rightarrow 4f$) transitions for the oxygen, transition metal and rare-earth ions, respectively. In fact, the specificity to the initial state symmetry is so large, that one does not need a very good energy resolution in order to measure which of the possible initial state symmetries is occupied, since different symmetries lead to completely different multiplet structured spectra. In other words, an experimental energy resolution of 500 meV is often enough to distinguish initial states that are different by not more than a few meV or less in energy, making the technique extremely valuable for the study of phase transitions which usually occur in the temperature range up to roughly room temperature (kT = 25 meV).

1.3 Challenges for theory

In the following, we will address two long standing topics in the research field of strongly correlated transition metal oxides, namely the spin-state transition in $LaCoO_3$ and the electronic structure of NiO. Synchrotron based spectroscopic experiments are presented. The results on the first topic show how crucial it is to take the full multiplet theory into account in order to be able to understand the magnetic properties of a partially filled t_{2g} material, while the results from the second topic provide a clear cut example how on-site multiplet structures could be affected by band formation. These experimental results illustrate the challenges faced by ab-initio based theories, namely to describe accurately both the (near) ground state properties and excitation spectra of strongly correlated transition metal oxides. We hope that LDA+DMFT and its extensions will provide a further major contribution in this research field.

2 Spin-state transition in $LaCoO_3$

2.1 Introduction

$LaCoO_3$ shows a gradual non-magnetic to magnetic transition with temperature, which has been interpreted originally four decades ago as a gradual population of high spin (HS, $t_{2g}^4 e_g^2$, $S = 2$) excited states starting from a low spin (LS, t_{2g}^6, $S = 0$) ground state [23–30]. This interpretation continued to be the starting point for experiments carried out up to roughly the first half of the 1990's [31–34]. All this changed with the theoretical work in 1996 by Korotin *et al.*, who proposed on the basis of local density approximation + Hubbard U (LDA+U) band structure calculations, that the excited states are of the intermediate spin (IS, $t_{2g}^5 e_g^1$, $S = 1$) type [35]. Since then many more studies have been carried out on $LaCoO_3$ with the majority of them [36–49] claiming to have proven the presence of this IS mechanism. In fact, this LDA+U work is so influential [50] that it forms the basis of most explanations for the fascinating properties of the recently synthesized layered cobaltate materials, which show giant magneto resistance as well as metal-insulator and ferro-ferri-antiferro-magnetic transitions with various forms of charge, orbital and spin ordering [51, 52]. There have been several attempts made since 1996 in order to revive the LS-HS scenario [53–57], but these were overwhelmed by the above mentioned flurry of studies claiming the IS mechanism [36–49]. Moreover, a new investigation using inelastic neutron scattering (INS) has appeared in [58] making again the claim that the spin state transition involves the IS states. In the following we describe our soft X-ray absorption spectroscopy (XAS) and magnetic circular dichroism (MCD) experiments at the Co-$L_{2,3}$ edge [59] to evaluate the validity of the various scenarios.

2.2 Experimental

Single crystals of $LaCoO_3$ have been grown by the traveling floating-zone method in an image furnace. The magnetic susceptibility was measured using a Quantum Design vibrating sample magnetometer (VSM), reproducing the data reported earlier [41]. The Co-$L_{2,3}$ XAS measurements were performed at the Dragon beamline of the National Synchrotron Radiation Research Center (NSRRC) in Taiwan with an energy resolution of 0.3 eV. The MCD spectra were collected at the ID08 beamline of the European Synchrotron Radiation Facility (ESRF) in Grenoble with a resolution of 0.25 eV and a degree of circular polarization close to 100% in a magnetic field of 6 Tesla. Clean sample areas were obtained by cleaving the crystals *in-situ* in chambers with base pressures in the low 10^{-10} mbar range. The Co-$L_{2,3}$ spectra were recorded using the total electron yield method (TEY). O-K XAS spectra were collected by both the TEY and the bulk sensitive fluorescence yield (FY) methods, and the close similarity of the spectra taken with these two methods verifies that the TEY spectra are representative for the bulk material. A CoO single crystal is measured *simultaneously* in a separate chamber to obtain relative energy referencing with better than a few meV accuracy, sufficient to extract reliable MCD spectra.

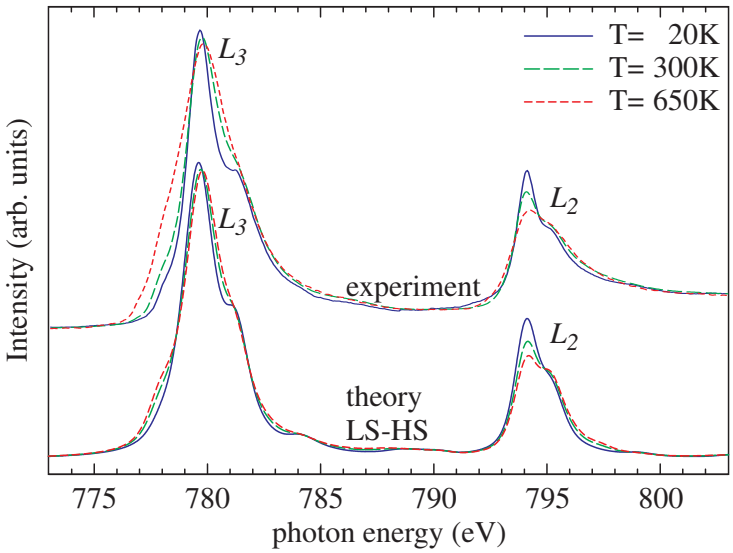

Fig. 1: *Experimental Co-$L_{2,3}$ XAS spectra taken from $LaCoO_3$ at various temperatures between 20 and 650 K, together with the corresponding theoretical isotropic spectra calculated using a CoO_6 cluster in the LS-HS scenario. For clarity, only the 20, 300 and 650 K spectra are shown.*

2.3 Results: XAS

Fig. 1 shows the set of Co-$L_{2,3}$ XAS spectra of $LaCoO_3$ taken for a wide range of temperatures. The set is at first sight similar to the one reported earlier [61], but it is in fact essentially different in details. First of all, our set includes a low temperature (20 K) spectrum representative for the LS state, and second, our spectra do not show a pronounced shoulder at 777 eV photon energy which is characteristic for the presence of Co^{2+} impurities [62]. The extended temperature range and especially the purity of the probed samples provide the required sensitivity for the spin-state related spectral changes.

The spectra are dominated by the Co $2p$ core-hole spin-orbit coupling which splits the spectrum roughly in two parts, namely the L_3 ($h\nu \approx 780$ eV) and L_2 ($h\nu \approx 796$ eV) white lines regions. The line shape of the spectrum depends strongly on the multiplet structure given by the Co $3d$-$3d$ and $2p$-$3d$ Coulomb and exchange interactions, as well as by the local crystal fields and the hybridization with the O $2p$ ligands. Unique to soft X-ray absorption is that the dipole selection rules are very effective in determining which of the $2p^5 3d^{n+1}$ final states can be reached and with what intensity, starting from a particular $2p^6 3d^n$ initial state (n=6 for Co^{3+}) [20, 21]. This makes the technique extremely sensitive to the symmetry of the initial state, e.g., the spin state of the Co^{3+} [52].

2.4 Analysis

We now simulate the spectrum of a Co^{3+} ion in the LS state using the successful configuration interaction cluster model that includes the full atomic multiplet theory and the hybridization with the O $2p$ ligands [20–22]. The CoO_6 cluster is taken to have the octahedral symmetry and the parameters are the same as the ones which succesfully reproduce the spectrum of LS

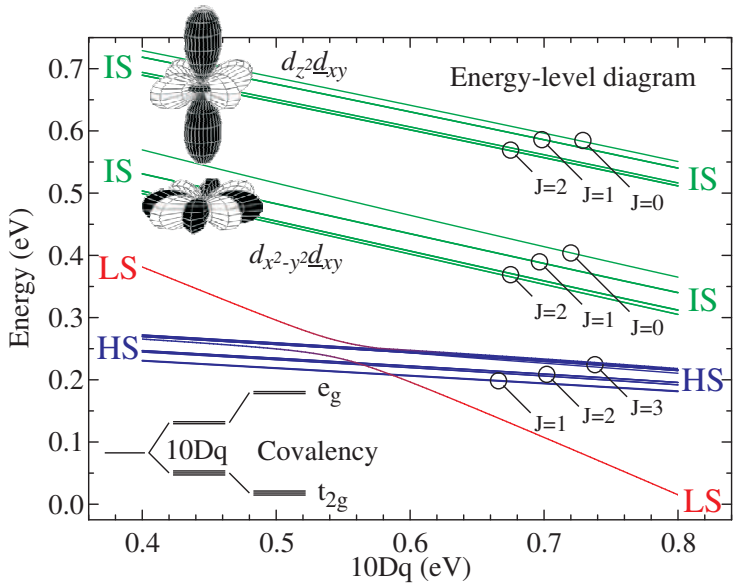

Fig. 2: *Energy level diagram of a CoO_6 cluster [63] as a function of the ionic part of the crystal field splitting* $10Dq$.

$EuCoO_3$ [52,63]. The result with the ionic part of the crystal field splitting set at $10Dq = 0.7$ eV is shown in Fig. 1 and fits well the experimental spectrum at 20 K.

Next we analyze the spectra for the paramagnetic phase. We use the same cluster keeping the O_h' symmetry, and calculate the total energy level diagram as a function of $10Dq$, see Fig. 2. We find that the ground state of the cluster is either LS or HS (and never IS) with a cross-over at about $10Dq = 0.58$ eV [64]. We are able to obtain good simulations for the spectra at all temperatures, see Fig. 1, provided that they are made from an incoherent sum of the above mentioned LS cluster spectrum calculated with $10Dq = 0.7$ eV and a HS cluster spectrum calculated with $10Dq = 0.5$ eV. It is not possible to fit the entire temperature range using one cluster with one particular temperature-independent $10Dq$ value for which the ground state is LS-like and the excited states HS-like. Moreover, each of these two $10Dq$ values have to be sufficiently far away from the LS-HS crossover point to ensure a large enough energy separation between the LS and HS so that the two do not mix due to the spin-orbit interaction. Otherwise, the calculated low temperature spectrum, for instance, will disagree with the experimental one. All this indicates that $LaCoO_3$ at finite temperatures is an inhomogeneous mixed spin state system.

The temperature dependence has been fitted by taking different ratios of LS and HS states contributing to the spectra. The extracted HS percentage as a function of temperature is shown in Fig. 3a. The corresponding effective activation energy is plotted in Fig. 3b. It increases with temperature and varies between 20 meV at 20 K to 80 meV at 650 K, supporting a recent theoretical analysis of the thermodynamics [57]. Here we would like to point out that these numbers are of the order k_BT and reflect total energy differences which include lattice relaxations [57] as sketched in the inset of Fig. 3b. Without these relaxations, we have for the LS state ($10Dq = 0.7$ eV) an energy difference of at least 50 meV between the LS and the HS as

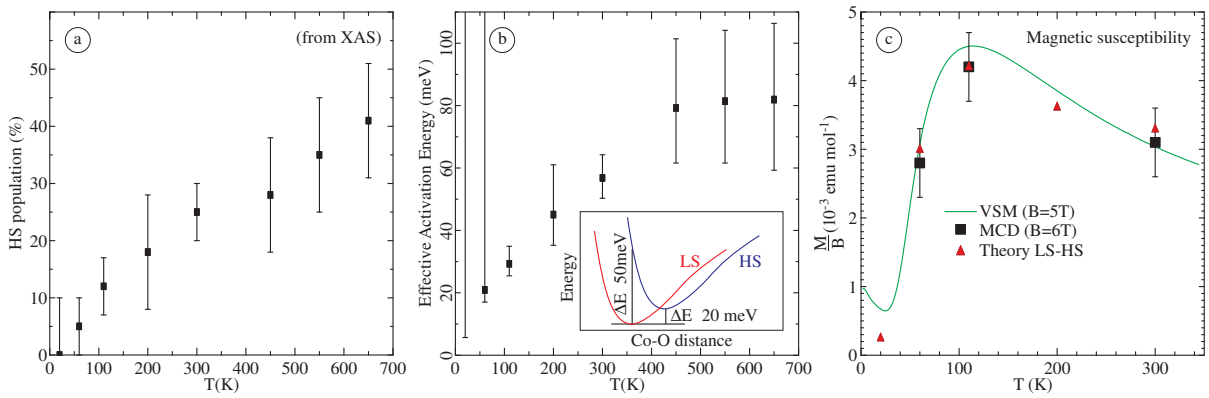

Fig. 3: *(a) The percentage of the HS population as obtained from the XAS data. (b) Corresponding effective activation energy between the LS and the lowest HS state. The inset sketches the role of lattice relaxations. (c) Magnetic susceptibility measured by VSM (solid line), calculated from the cluster (red triangles) using the HS population of (a), and extracted from MCD data (black squares) of Fig. 4.*

shown in Fig. 2. In such a frozen lattice, the energy difference is larger than $k_B T$. It is also so large that the ground state is indeed highly pure LS as revealed by the 20 K spectrum.

To check the validity of our analysis, we calculate the magnetic susceptibility using the CoO_6 cluster and the HS occupation numbers from Fig. 3 as derived from the XAS data. The results are plotted in Fig. 3c (red triangles) together with the magnetic susceptibility as measured by the VSM (solid line). We can observe clearly a very good agreement: the magnitude and its temperature dependence is well reproduced. This provides another support that the spin-state transition is inhomogeneous and involves lattice relaxations. A homogeneous LS-HS model, on the other hand, would produce a much too high susceptibility if it is to peak at 110 K [33, 34, 36, 41]. In addition, it is crucial to realize that the Van Vleck contribution to the magnetic susceptibility strongly depends on the intermixing between the LS and HS states. It is precisely this aspect which also sets the condition that the energy separation between the LS and HS states in the cluster should be larger than 50 meV, otherwise the calculated Van Vleck contribution would already exceed the experimentally determined total magnetic susceptibility at low temperatures. This in fact is a restatement of the above mentioned observation that the low temperature spectrum is highly pure LS.

2.5 Results: MCD

To further verify the direct link between the spectroscopic and the VSM magnetic susceptibility data, we carried out MCD experiments on $LaCoO_3$ at 60, 110 and 300 K, i.e. in the paramagnetic phase, using a 6 Tesla magnet. Fig. 4 shows XAS spectra taken with circularly polarized soft-X-rays with the photon spin parallel and antiparallel aligned to the magnetic field. The difference in the spectra using these two alignments is only of the order of 1%, but can nevertheless be measured reliably due to the good signal to noise ratio, stability of the beam, and the accurate photon energy referencing. The difference curves are drawn in the middle of Fig. 4 with a

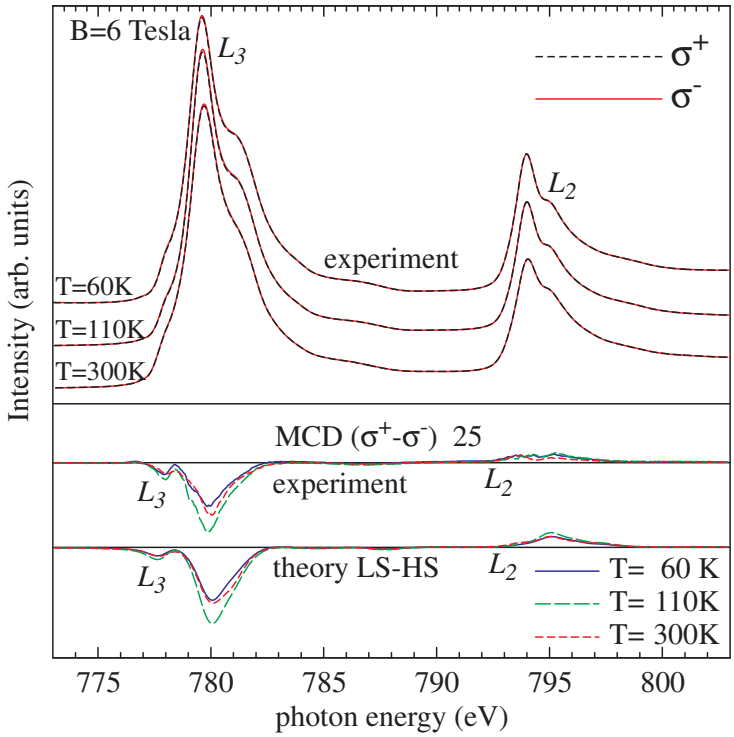

Fig. 4: *Top curves: experimental Co-$L_{2,3}$ XAS spectra taken from $LaCoO_3$ at 60, 110, and 300 K using circularly polarized X-rays with the photon spin aligned parallel (black dotted line, σ^+) and antiparallel (red solid line, σ_-) to the 6 Tesla magnetic field. Middle curves: experimental MCD spectra defined as the difference between the two spin alignments. Bottom curves: theoretical MCD spectra calculated in the LS-HS scenario.*

magnification of 25x. Hereby we have subtracted a small signal due to the presence of about 1.5% Co^{2+} impurities. We also plotted the simulated MCD spectra from the cluster model within the LS-HS scenario, and we can clearly observe a very satisfying agreement with the experiment. Alternatively, using the MCD sum-rules developed by Thole and Carra et al. [65, 66], we can extract directly the orbital (L_z) and spin ($2S_z$) contributions to the induced moments without the need to do detailed modeling [67]. This result normalized to the applied magnetic field is plotted in Fig. 3c, and we can immediately observe the close agreement with the VSM data.

An important aspect that emerges directly from the MCD experiments, is the presence of a very large induced orbital moment: we find that $L_z/S_z \approx 0.5$. This means that the spin-orbit coupling (SOC) must be considered in evaluating the degeneracies of the different levels, as is done for the energy level diagram in Fig. 2. Let us discuss the consequences for the HS state. We see that the 15-fold degenerate (3-fold orbital and 5-fold spin) HS state is split by the SOC. A t_{2g} electron has a pseudo orbital momentum of $\tilde{L}$=1 [68] which couples with the spin to a pseudo total momentum of $\tilde{J}$=1, 2, or 3. The $\tilde{J}$=1 triplet is the lowest in energy and we find from our cluster that this state has L_z=0.6 and S_z=1.3, in good agreement with the experimental $L_z/S_z \approx 0.5$. Realizing that this state is a triplet with a spin momentum (S_z) so close to 1, it is no wonder that many studies incorrectly interpreted this state as an IS state. Its expectation

value for the spin ($\langle S^2 \rangle = S(S+1)$) is however very close to 6 and the formal occupation numbers of the d_{z^2} and the $d_{x^2-y^2}$ orbitals are both equal to 1. This state is clearly a HS state and should not be confused with an IS state. We find a g-factor of 3.2, in good agreement with the values found from ESR [54, 56] and INS data [60].

2.6 Discussion

We have shown so far that the spin state transition in $LaCoO_3$ is in very good agreement with a LS–HS picture. The question now remains if it could also be explained within a LS–IS scenario. For that we first have to look what the IS actually is. The IS state has one hole in the t_{2g} shell and one electron in the e_g shell. Due to the strong orbital dependent Coulomb interactions, the strong-Jahn-Teller states of the type $d_{z^2}\underline{d}_{xy}$ and their x, y, z-cyclic permutations have much higher energies than the weak-Jahn-Teller $d_{x^2-y^2}\underline{d}_{xy}$ plus cyclic permutations. Here the underline denotes a hole (see Fig. 2). These weak-Jahn-Teller states indeed form the basis for the orbital ordering scheme as proposed for the IS scenario by Korotin *et al.* [35]. However, these real-space states do not carry a large orbital momentum, and are therefore not compatible with the values observed in the MCD measurements. Likewise, the strong Jahn-Teller-like local distortions in the IS state proposed by Maris *et al.* [46] would lead to a quenching of the orbital momentum. We therefore can conclude that the IS scenarios proposed so far have to be rejected on the basis of our MCD results. Moreover, an IS state would lead in general to a much larger van Vleck magnetism than a HS state. This is related to the fact that the LS state couples directly to the IS via the SOC, while the HS is not. To comply with the measured low temperature magnetic susceptibility, the energy difference between the LS and IS has to be 150 meV at least, making it more difficult to find a mechanism by which the maximum of the susceptibility occurs at 110 K. Finally, within the LS-IS scenario, we were not able to find simulations which match the experimental XAS and MCD spectra.

To summarize, we provide unique spectroscopic evidence that the spin state transition in $LaCoO_3$ can be well described by a LS ground state and a triply degenerate HS excited state, and that an inhomogeneous mixed-spin-state system is formed. The large orbital momentum revealed by the MCD measurements invalidates existing LS-IS scenarios. A consistent picture has now been achieved which also explains available magnetic susceptibility, ESR and INS data.

3 Electronic structure of NiO

3.1 Introduction

NiO is a benchmark system in solid state physics. It crystallizes in the NaCl structure, has a partially filled $3d$ shell (Ni^{2+} d^8), and is an antiferromagnetic insulator with a Néel temperature of 523 K [69]. It was pointed out early on by de Boer and Verwey [70] that many of the properties of the $3d$ transition metal compounds do not agree with the predictions of band theory, e.g., standard band theory predicts NiO to be metallic. A qualitative explanation was proposed

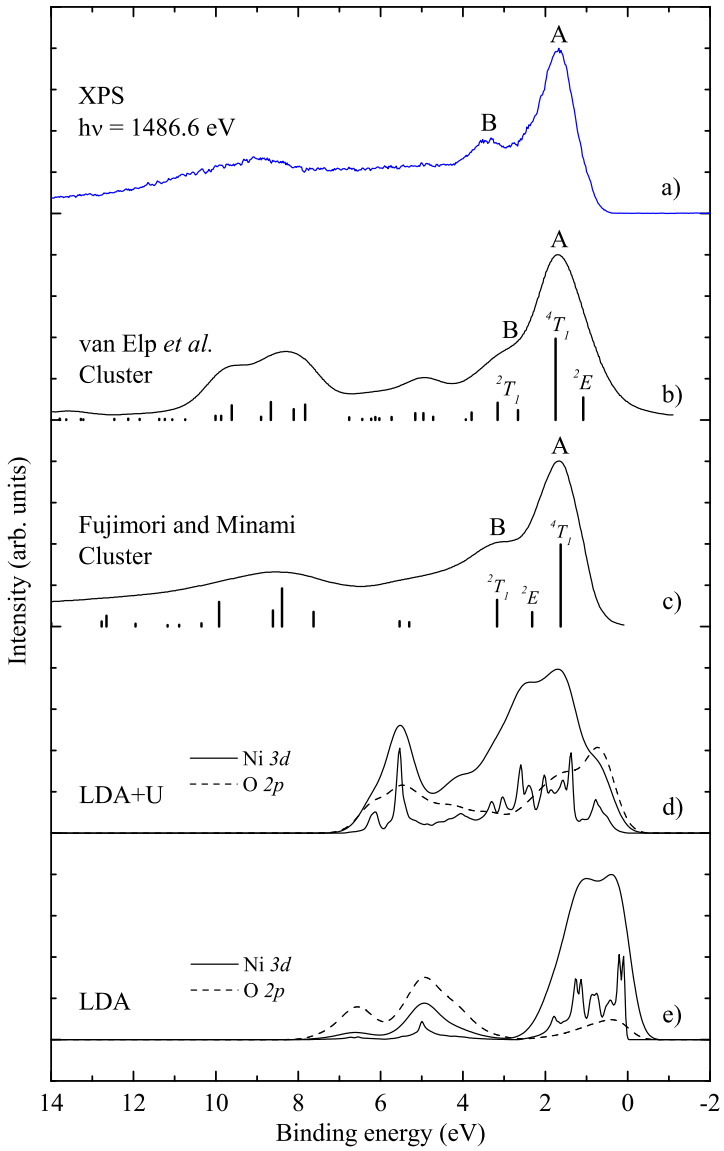

Fig. 5: *Valence band XPS (1486.6 eV) spectrum of an in situ cleaved NiO single crystal. The results of two single-site cluster calculations (reproduced from Refs. 79 and 80), and LDA and LDA+U calculations are also included for comparison.*

in terms of the Mott-Hubbard model [71,72] in which the on-site Ni $3d$-$3d$ Coulomb interaction plays a decisive role.

An early *ab initio* attempt to fix the shortcoming of band theory was to treat NiO as a Slater insulator in which the doubling of the unit cell allows for the existence of a gap [73–75]. However, the calculated gap of about 0.2 eV [73] turned out to be much too small: A combined photoemission (PES) and bremsstrahlung-isochromat (BIS) spectroscopy study showed that the band gap is 4.3 eV [76] and established thereby the correlated nature of NiO. The inclusion of a self-interaction-correction (SIC) or Hubbard U term to the density-functional formalism may provide a justification for the magnitude of the experimental band gap [77, 78].

Yet, one of the most direct methods to critically test the accuracy of the different approaches,

is to determine the excitation spectrum associated with the introduction of an extra particle into the system [81]. Curve (a) in Fig. 5 displays the valence band X-ray photoemission spectrum (XPS, $h\nu$ = 1486.6 eV) of an *in situ* cleaved NiO single crystal. This spectrum represents essentially the Ni $3d$ spectral weight since the photoionization cross section of the O $2p$ is relatively small [82]. One can clearly observe from curve (e) in Fig. 5 that the Ni $3d$ density of states calculated by band theory (in the local density approximation, LDA) does not match at all: It has a Fermi cut-off and the line shape is completely different. The inclusion of the Hubbard U in the calculations (LDA+U) does not solve the line shape problem, see curve (d). All this demonstrates the shortcomings of mean field theories to describe spectra associated with the fundamental one-particle Green's function of the system [78, 83].

A completely different approach is to give up the translational symmetry of the system in order to focus on the local correlations and, especially, the dynamics of the propagation of the injected particle. Curve (c) of Fig. 5 shows the Ni $3d$ spectral weight from an early cluster configuration-interaction calculation by Fujimori and Minami [80], which also includes the full atomic multiplet theory. The agreement with the experimental spectrum is extremely good. Nevertheless, a later cluster calculation by van Elp *et al.* [79] arrived at a less satisfactory result: Peak B has almost disappeared in the calculation, see curve (b). The prime motivation to use a different set of model parameters here is to infer that the first ionization state is low spin (^2E) [84] rather than the Hund's rule high spin (^4T), analogous to the case of Zhang-Rice singlets in the cuprates [85, 86]. Recent developments combining LDA with dynamical mean field [87–90] or GW approaches [91] yield Ni $3d$ spectral weights which deviate in important details from the experimental spectrum. These discrepancies between the experiment and the later theoretical simulations [79, 87–90] do not provide confidence that one has made progress in understanding the nature of the first ionization state.

The issues that we need to address now are threefold. First of all we have to establish whether the XPS valence band spectrum in Fig. 5 is truly representative for bulk NiO. There are reports in the literature claiming that certain satellite peaks in the Ni $2p$ spectrum are due to surface effects [92–95]. Second, we have to determine to what extent a single-site many body approach can be utilized to describe the electronic structure of NiO for which band formation is also essential. Third, we need to identify the nature of the first ionization state in the framework of a local *ansatz*. To this end we measured the valence band of NiO utilizing the more bulk-sensitive hard X-ray photoelectron spectroscopy (HAXPES) and we investigated experimentally the electronic structure of NiO impurities in MgO [96].

3.2 Experimental

The XPS data ($h\nu = 1486.6$ eV) on *in situ* cleaved NiO single crystals were recorded using a Vacuum Generators twin crystal monochromator Al-K_α source and an Scienta SES-100 analyzer, with an overall energy resolution set to 0.35 eV. The HAXPES data ($h\nu = 6500$ eV) were taken at the Taiwan beamline BL12XU of SPring-8 in Hyogo, Japan using an MBS A-1HE analyzer. The overall energy resolution was set to 0.35 eV. The NiO impurity in MgO system

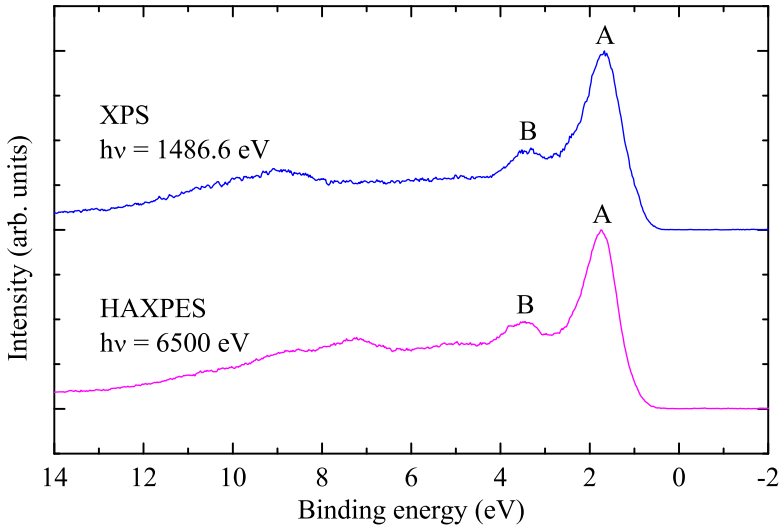

Fig. 6: *Valence band photoemission spectra of an in situ cleaved NiO single crystal recorded using 1486.6 eV (XPS) and 6500 eV (HAXPES) photons.*

was prepared *in situ* as 10-20 nm thin films on polycrystalline Ag by means of molecular beam epitaxy. The measurements were performed at the 11A1 Dragon beamline of the NSRRC in Hsinchu, Taiwan. The photoemission spectra were recorded at the Cooper minimum of Ag $4d$ ($h\nu = 140$ eV) [97] using a Scienta SES-100 analyzer with an overall energy resolution set at about 0.15 eV.

3.3 Results

In Fig. 6 we show the valence band photoemission spectra of a freshly cleaved NiO bulk crystal, taken with a photon energy of 1486.6 eV (XPS) and 6500 eV (HAXPES). By increasing the photon energy we increase also the kinetic energy of the outgoing photoelectron and, thus, also the inelastic mean free path. One can estimate that the probing depth is then enhanced from about 15 Å to roughly 80 Å [98]. We observe that the spectra are very similar. We, thus, conclude that the XPS data as displayed in Figs. 5 and 6 is representative for the NiO bulk material and that the contribution of surface effects [92–95] can be safely neglected. To be specific: Peak B is intrinsic for bulk NiO. We would like to note that increasing the photon energy from 1486.6 eV to 6500 eV does not alter much the Ni $3d$ character of the spectrum. The O $2p$ photoionization cross section relative to that of the Ni $3d$ remains very small, it changes from 1/13 to only 1/10 [82], meaning that peak B truly belongs to the Ni $3d$ spectral weight and not to the O $2p$ [89].

The valence band spectrum of the $Ni_{0.05}Mg_{0.95}O$ impurity system is shown in Fig. 7 together with the spectrum of an MgO reference thin film grown simultaneously under identical oxygen and substrate conditions. The $Ni_{0.05}Mg_{0.95}O$ film (and also the MgO film) was capped by 2 monolayers of MgO in order to prevent the surface termination to have an effect on the local electronic structure of the Ni impurity. The inset in the figure displays the Ni $L_{2,3}$ X-ray absorption spectra of the $Ni_{0.05}Mg_{0.95}O$ and the NiO bulk. The spectra are essentially identical,

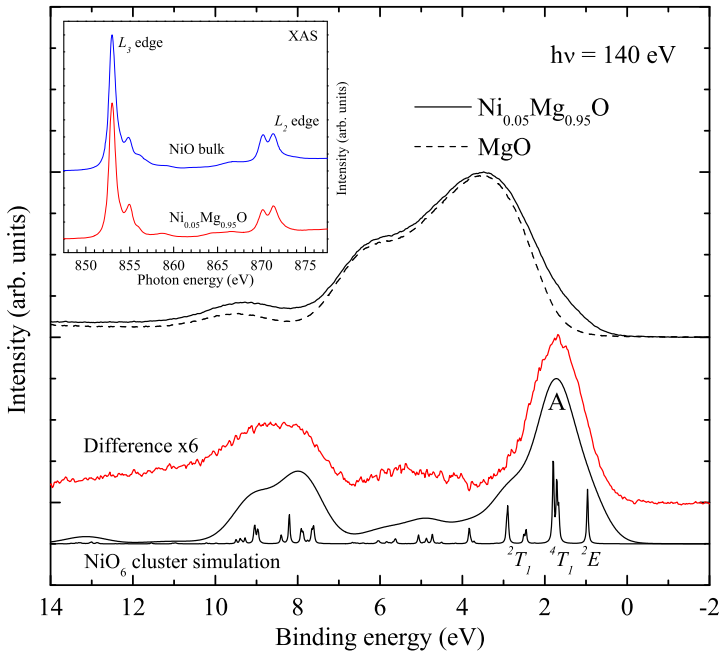

Fig. 7: *Extraction of the NiO impurity valence band photoemission spectrum: Valence band spectra of $Ni_{0.05}Mg_{0.95}O$ and an MgO reference, together with the resulting difference spectrum. Also included is the result of a single-site NiO_6 configuration-interaction cluster calculation. The inset shows the Ni $L_{2,3}$ X-ray absorption spectrum of the $Ni_{0.05}Mg_{0.95}O$ together with that of bulk NiO.*

verifying that the Ni in the $Ni_{0.05}Mg_{0.95}O$ has very similar local surrounding (NiO_6 octahedra) as in the bulk.

The valence band spectra of the $Ni_{0.05}Mg_{0.95}O$ and MgO systems are normalized to their O $2s$ core level intensities. Both are dominated by the O $2p$ valence band, yet, there are clear differences between them due to the presence or absence of the 5% NiO impurity. The difference spectrum multiplied by a factor of 6 is given by the red curve in Fig. 7. The line shape remains the same for films with lower Ni concentrations, as is the case for that of the Ni $2p$ [99]. This curve represents essentially the Ni $3d$ spectral weight of the NiO impurity since the photoionization cross section of the Ni $3d$ is an order of magnitude larger than that of the O $2p$ at the photon energy used [82]. Remarkable is that it is different from the spectrum of bulk NiO as shown in Figs. 5 and 6. The impurity spectrum lacks specifically peak B which is prominently present in the bulk spectrum.

3.4 Analysis

To interpret and understand the impurity spectrum, we have performed simulations using the well-proven configuration-interaction cluster model which includes the full atomic multiplet theory [22, 20, 21]. The simulations have been carried out for a NiO_6 cluster using the program XTLS 8.3 [22].

The bottom curve in Fig. 7 shows the Ni $3d$ one-electron removal spectrum from the cluster

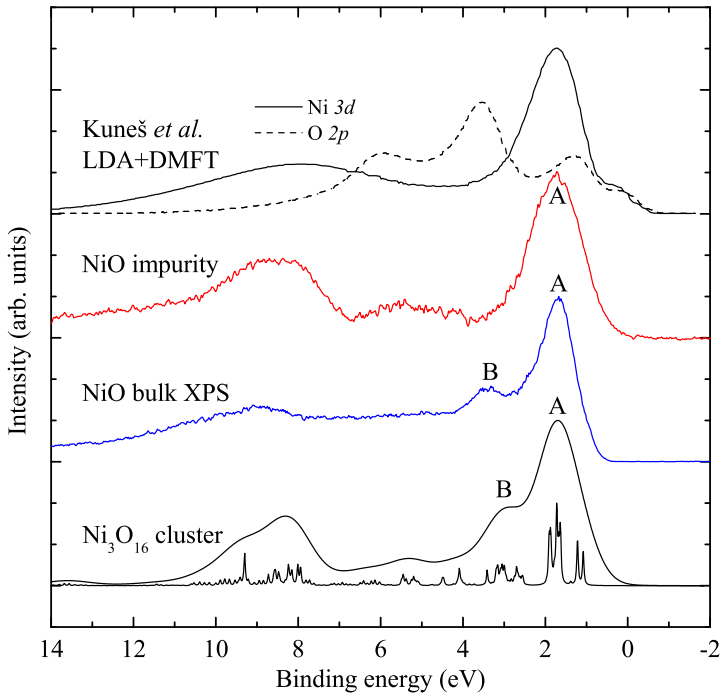

Fig. 8: *Comparison of the valence band photoemission spectra of bulk NiO and NiO impurity in MgO. Also included is the simulated Ni* $3d$ *and O* $2p$ *spectral weights of the NiO valence band from a LDA+DMFT calculation (reproduced from Ref. 89) and the result of a three-site* Ni_3O_{16} *configuration-interaction cluster calculation.*

calculation. The agreement with the experiment is very satisfactory. In order to achieve this, we have started the calculations by using parameter values which were suggested from earlier studies on NiO [79, 22, 100, 101]. We then fine-tune the parameters describing the octahedral crystal and ligand fields, and also the difference between the Hubbard U and the O $2p$-Ni $3d$ charge transfer energy [102]. The crucial issue here is to obtain a main line (peak A) without having another feature appearing at about 2 eV higher energies (peak B) as was the case in the simulations by Fujimori and Minami [80] and by van Elp *et al.* [79]. This has implications for the energetics of the states making up the valence band as we explain in the following.

A detailed look at the cluster calculations displayed in Fig. 5 shows that peak A is given by the ${}^4T_1$ final state of the Ni $3d^7$ multiplet structure while peak B is due to the ${}^2T_1$. Avoiding the appearance of peak B means that the energy splitting between these two states must be made smaller, e.g., 1 eV or less. This is what we have done in our simulation in Fig. 7, using different but equally reasonable parameter values [102]. The consequences for the physics are quite far reaching. Given the fact that various X-ray absorption studies find an effective octahedral crystal and ligand field splitting of about 1.65 eV [100, 101], i.e., the splitting between the isospin ${}^2T_1$ and ${}^2E$ states, we arrive at the conclusion that the ${}^2E$ must be lower in energy than the ${}^4T_1$ by 0.65 eV or more. This is what we read from our results in Fig. 7. In other words, our impurity study provides the spectroscopic evidence that the first ionization state has a compensated-spin character rather than the Hund's rule high-spin. This in turn justifies that the ground state of a hole doped NiO system may indeed be low-spin in nature [84].

We now return to the problem of the bulk NiO valence band spectrum. Fig. 8 shows the Ni $3d$ spectral weight taken with XPS and compares it with the spectra of the NiO impurity and of the single-site LDA+DMFT calculation [89]. One can clearly observe that peak B is absent in the impurity as well as in the Ni $3d$ spectral weight of the single-site calculation. In fact, one could infer that the calculation reproduces quite well the impurity spectrum, with perhaps some discrepancies due to the incomplete implementation of the multiplet structure of the on-site Coulomb interactions. Yet, the discrepancy with the bulk spectrum strongly suggests that the origin of peak B must be sought in non-local correlations, i.e., effects which cannot be included in a single-site approach.

3.5 Non-local screening

Our suggestion is that peak B is due to non-local screening processes involving the formation of low-energetic coherent many body states on neighboring NiO clusters, which are of the ^2E type as we have shown above. The mechanism is analogous as proposed earlier for the Ni $2p$ core level spectrum of bulk NiO [103], but the application of it for the valence band is only valid for local states which are relatively stable against band formation. This may not be applicable for the ^2E state, which is a state in which a hole is injected in an e_g orbital starting from the $3d^8$ $^3A_2$ ground state [101]. This hole can be expected to readily propagate in the lattice since the hopping between the Ni $3d(e_g)$ and O $2p(\sigma)$ orbitals are rather large [79, 103], yet, it may leave behind an energetically costly wake of wrong spins in the antiferromagnetic lattice. In any case, it would not be meaningful to describe its band formation as a low-energy screening process involving neighboring ^2E states [104].

However, for the main peak of the bulk NiO spectrum, i.e., the $^4T_1$ state, we infer that we can make a meaningful approximation by using the coherent ^2E screening model. The $^4T_1$ consists of a hole injected into the t_{2g} orbital, and its ability to move is rather limited since the overlap between the Ni $3d(t_{2g})$ and O $2p(\pi)$ is small. One could consider the $^4T_1$ as a localized quasi-core state. We then can invoke the non-local screening process as follows: After the creation of the $^4T_1$ state, an e_g electron from a neighboring NiO cluster hops onto the Ni site, leaving behind a coherent ^2E hole state on that neighbor. A sketch for this process is given in Fig. 9. These two states are energetically almost degenerate [103], and the Ni $3d(e_g)$ and O $2p(\sigma)$ hybridization between them is then strong enough to produce two peaks: Not only the main peak A but also the satellite peak B.

3.6 Multi-site analysis

To confirm our assignments, Tanaka [96] has performed a Ni_3O_{16} cluster calculation consisting of three edge-shared NiO_6 octahedra. While all the O $2p$ and Ni $3d$ orbitals are included for the NiO_6 octahedron in the center where the photo-excitation takes place, those on the other parts of the cluster are replaced by a reduced basis set using the method in Ref. [105]. The results are displayed in Fig. 8 and demonstrate the presence of both peaks A and B. Note that the same parameters have been used as for the single-site calculation which produces only peak

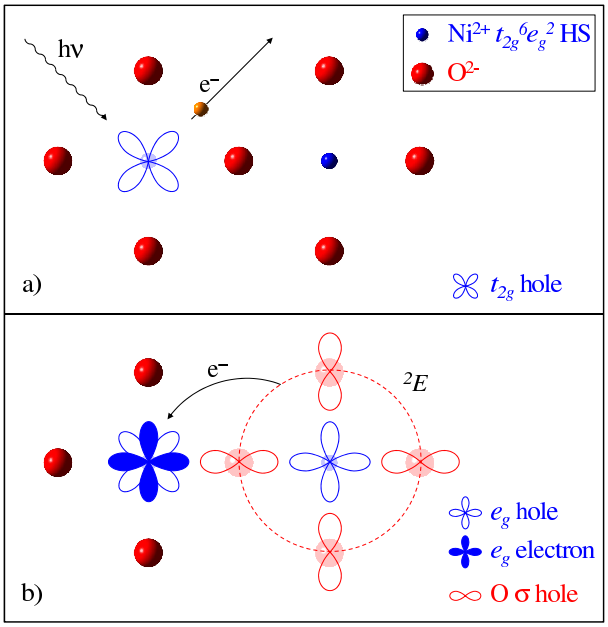

Fig. 9: *Non-local screening in valence band photoemission on NiO: (a) Creation of the atomic-like (quasi-core)* ${}^4T_1$ *hole state by the photoemission process. (b) Screening by a next nearest neighbor* NiO_6 *cluster producing a coherent low-energetic* ${}^2E$ *hole state there.*

A, see Fig. 7. We also note that the energy difference between peaks A and B is somewhat smaller and the intensity of peak B is slightly larger than those of the experiments. This can be explained by the fact that the number of neighboring Ni sites is only two in the Ni_3O_{16} cluster: the energy difference will increase and the intensity of peak B will decrease for a larger number of neighboring sites [105].

3.7 Conclusion

To summarize: We have succeeded to determine reliably the Ni $3d$ valence band spectra representative for bulk NiO as well as for NiO as an impurity system. From the impurity data we are able to extract the local electronic structure and the correlations herein, thereby establishing firmly the compensated-spin character of the first ionization state. By comparing the bulk with the impurity system, we were able to identify features in the bulk NiO spectrum which are caused by screening processes involving local quasi-core valence band states and non-local low-energetic many body states.

Acknowledgement

The research is supported by the Deutsche Forschungsgemeinschaft through SFB608 and FOR 1346. We gratefully acknowledge the NSRRC, ESRF, and SPring-8 staff for providing us with beamtime. We would like to thank L. Hamdan for her skillful technical and organizational assistance and J. Weinen for his assistance in preparing this manuscript.

References

[1] for a review see: Electronic Conduction in Oxides by N. Tsuda, K. Nasu, A. Yanase, and K. Siratori, Springer Series in Solid-State Sciences 94, (Springer Verlag, Berlin 1991)

[2] for a review see: M. Imada, A. Fujimori, and Y. Tokura, Rev. Mod. Phys. **70**, 1039 (1998)

[3] R.J. Birgenau and M.A. Kastner, Science **288**, 437 (2000)

[4] Y. Tokura and N. Nagaosa, Science **288**, 462 (2000)

[5] J. Orenstein and A.J. Millis, Science **288**, 468 (2000)

[6] for a review see: A.P. Ramirez, J. Phys.: Conden. Matter **9**, 8171 (1997)

[7] D.I. Khomskii and G.A. Sawatzky, Solid State Commun. **102**, 87 (1997)

[8] T. Mizokawa and A. Fujimori, Phys. Rev. B **51**, 12880 (1995); Phys. Rev. B **54**, 5368 (1996); Phys. Rev. B **56**, R493 (1997)

[9] A.A. Taskin, A.N. Lavrov, and Yoichi Ando, Phys. Rev. Lett. **90**, 227201 (2003)

[10] A. Maignan, C. Martin, D. Pelloquin, N. Nguyen, and B. Raveau, J. Solid State Chem. **142**, 247 (1999)

[11] J.-H. Park, L.H. Tjeng, J.W. Allen, C.T. Chen, P. Metcalf, J.M. Honig, F.M.F. de Groot, and G.A. Sawatzky, Phys. Rev. B **61**, 11506 (2000)

[12] S.Y. Ezhov, V.I. Anisimov, D.I. Khomskii, and G.A. Sawatzky, Phys. Rev. Lett. **83**, 4136 (1999)

[13] F. Mila, R. Shiina, F.-C. Zhang, A. Joshi, M. Ma, V.I. Anisimov, and T.M. Rice, Phys. Rev. Lett. **85**, 1714 (2000)

[14] C. J. Ballhausen, *Introduction to Ligand Field Theory* (McGraw-Hill, New York, 1962)

[15] S. Sugano, Y. Tanabe, and H. Kamimura, *Multiplets of Transition-Metal Ions in Crystals* (Academic, New York, 1970)

[16] M.W. Haverkort, PhD thesis, University of Cologne (2005), chapter 1, arXiv:cond-mat/0505214

[17] for a review see: 'Photoelectron Spectroscopy' by S. Hüfner, Springer Series in Solid-State Sciences 82, (Springer Verlag, Berlin 1996)

[18] for a review see: 'Unoccupied Electronic States', 'Fundamentals for XANES, EELS, IPS, and BIS', edited by J.C. Fuggle and J.E. Inglesfield, Topics in Applied Physics, Vol. 69 (Springer Verlag, Berlin 1992)

[19] C. T. Chen and F. Sette, Phys. Scr. **T31**, 119 (1990)

[20] See review by F. M. F. de Groot, J. Electron Spectrosc. Relat. Phenom. **67**, 529 (1994)

[21] See review in the Theo Thole Memorial Issue,
J. Electron Spectrosc. Relat. Phenom. **86**, 1 (1997)

[22] A. Tanaka and T. Jo, J. Phys. Soc. Jpn. **63**, 2788 (1994)

[23] R.R. Heikes, R.C. Miller, and R. Mazelsky, Physica **30**, 1600 (1964)

[24] G. Blasse, J. Appl. Phys. **36**, 879 (1965).

[25] C. S. Naiman *et al.*, J. Appl. Phys. **36**, 1044 (1966)

[26] G. H. Jonker, J. Appl. Phys. **37**, 1424 (1966)

[27] J.B. Goodenough and P. M. Raccah, J. Appl. Phys. Suppl. **36**, 1031 (1965).

[28] P.M. Raccah and J.B. Goodenough, Phys. Rev. **155**, 932 (1967)

[29] J.B. Goodenough, in *Progress in Solid State Chemistry*, edited by H. Reiss
(Pergamon, Oxford, 1971), Vol. 5.

[30] V.G. Bhide, D.S. Rajoria, G. Rama Rao, and C.N.R. Rao, Phys. Rev. B **6**, 1021 (1972)

[31] K. Asai *et al.*, Phys. Rev. B **50**, 3025 (1994)

[32] M. Itoh, I. Natori, S. Kubota, and K. Motoya, J. Phys. Soc. Jpn. **63**, 1486 (1994)

[33] M. Itoh, M. Sugahara, I. Natori, and K. Motoya, J. Phys. Soc. Jpn. **64**, 3967 (1995)

[34] S. Yamaguchi, Y. Okimoto, H. Taniguchi, and Y. Tokura, Phys. Rev. B **53**, R2926 (1996)

[35] M. A. Korotin *et al.*, Phys. Rev. B **54**, 5309 (1996)

[36] T. Saitoh *et al.*, Phys. Rev. B **55**, 4257 (1997); *ibid.* **56**, 1290 (1997)

[37] S. Stølen *et al.*, Phys. Rev. B **55**, 14103 (1997)

[38] K. Asai *et al.*, J. Phys. Soc. Jpn. **67**, 290 (1998)

[39] J. Okamoto *et al.*, Phys. Rev. B **62**, 4455 (2000)

[40] P. Ravindran *et al.*, J. Appl. Phys. **91**, 291 (2002)

[41] C. Zobel *et al.*, Phys. Rev. B **66**, 020402(R) (2002)

[42] P. G. Radaelli and S.-W. Cheong, Phys. Rev. B **66**, 094408 (2002)

[43] T. Vogt, J.A. Hriljac, N.C. Hyatt, and P. Woodward, Phys. Rev. B **67**, 140401(R) (2003)

[44] I.A. Nekrasov, S.V. Streltsov, M.A. Korotin, and V.I. Anisimov, Phys. Rev. B **68**, 235113 (2003)

[45] D. Louca and J.L. Sarrao, Phys. Rev. Lett. **91**, 155501 (2003)

[46] G. Maris *et al.*, Phys. Rev. B **67**, 224423 (2003).

[47] A. Ishikawa, J. Nohara, and S. Sugai, Phys. Rev. Lett. **93**, 136401 (2004)

[48] M. Magnuson *et al.*, Europhys. Lett. **68**, 289 (2004)

[49] K. Knizek, P. Novak, and Z. Jirak, Phys. Rev. B **71**, 054420 (2005)

[50] The Korotin Phys. Rev. B 1996 paper has at present been cited for already more than 170 times.

[51] See List of References in Hu *et al*.

[52] Z. Hu *et al.*, Phys. Rev. Lett. **92**, 207402 (2004)

[53] M. Zhuang, W. Zhang, and N. Ming, Phys. Rev. B **57**, 10705 (1998)

[54] S. Noguchi, *et al.*, Phys. Rev. B **66**, 094404 (2002)

[55] T. Kyômen, Y. Asaka, and M. Itoh, Phys. Rev. B **67**, 144424 (2003)

[56] Z. Ropka and R.J. Radwanski, Phys. Rev. B **67**, 172401 (2003)

[57] T. Kyômen, Y. Asaka, and M. Itoh, Phys. Rev. B **71**, 024418 (2005)

[58] D. Phelan *et al.*, Phys. Rev. Lett. **96**, 027201 (2006).

[59] M.W. Haverkort, Z. Hu, J.C. Cezar, T. Burnus, H. Hartmann, M. Reuther, C. Zobel, T. Lorenz, A. Tanaka, N.B. Brookes, H.H. Hsieh, H.-J. Lin, C.T. Chen, and L.H. Tjeng, Phys. Rev. Lett. **97**, 176405 (2006)

[60] Z. Podlesnyak *et al.*, submitted to Phys. Rev. Lett. (LE10336/Podlesnyak)

[61] M. Abbate *et al.*, Phys. Rev. B **47**, 16124 (1993)

[62] S. I. Csiszar *et al.*, Phys. Rev. Lett. **95**, 187205 (2005)

[63] CoO_6 cluster parameters [eV]: Δ=2.0, $pd\sigma$=-1.7, U_{dd}=5.5, Slater integrals 80% of Hartree Fock values.

[64] In a pure ionic model, the LS-HS cross-over occurs at 10Dq $\approx$ 2.2 eV.

[65] B.T. Thole, P. Carra, F. Sette, and G. van der Laan, Phys. Rev. Lett. **68**, 1943 (1992)

[66] P. Carra, B.T. Thole, M. Altarelli, and X. Wang, Phys. Rev. Lett. **70**, 694 (1993)

[67] The sumrules gives numbers for L_z and $S_z + \frac{7}{2}T_z$; $T_z = 0$ for the HS state as justified from cluster calculations; the number of $3d$ holes is about 3.5.

[68] A. Abragam and B. Bleaney, *Electron paramagnetic resonance of transition ions* (Clarendon, Oxford, 1970)

[69] W.L. Roth, Phys. Rev., **110**, 1333 (1958)

[70] J.H. de Boer and E.J.W. Verwey, Proc. Phys. Soc. London, **49**, 59 (1937)

[71] N.F. Mott, Proc. Phys. Soc. London, Sect. A, **62**, 416 (1949)

[72] J. Hubbard, Proc. R. Soc. London, Ser. A, **276**, 238 (1963)

[73] T. Oguchi et al., Phys. Rev. B, **28**, 6443 (1983)

[74] K. Terakura et al., Phys. Rev. Lett., **52**, 1830 (1984)

[75] K. Terakura et al., Phys. Rev. B, **30**, 4734 (1984)

[76] G.A. Sawatzky and J.W. Allen, Phys. Rev. Lett., **53**, 2339 (1984)

[77] A. Svane and O. Gunnarsson, Phys. Rev. Lett., **65**, 1148 (1990)

[78] V.I. Anisimov et al., Phys. Rev. B, **44**, 943 (1991)

[79] J. van Elp et al., Phys. Rev. B, **45**, 1612 (1992)

[80] A. Fujimori and F. Minami, Phys. Rev. B, **30**, 957 (1984)

[81] C.-O. Almbladh and L. Hedin, *Handbook on Synchrotron Radiation*, edited by E. E. Koch, Vol. 1b (North-Holland, Amsterdam, 1983) p. 607

[82] M.B. Trzhaskovskaya et al., At. Data Nucl. Data Tables, **77**, 97 (2001)

[83] V.I. Anisimov et al., Phys. Rev. B, **48**, 16929 (1993)

[84] P. Kuiper et al., Phys. Rev. Lett., **62**, 221 (1989)

[85] F.C. Zhang and T.M. Rice, Phys. Rev. B, **37**, 3759 (1988)

[86] H. Eskes and G.A. Sawatzky, Phys. Rev. Lett., **61**, 1415 (1988)

[87] X. Ren et al., Phys. Rev. B, **74**, 195114 (2006)

[88] J. Kuneš et al., Phys. Rev. Lett., **99**, 156404 (2007)

[89] J. Kuneš et al., Phys. Rev. B, **75**, 165115 (2007)

[90] Q. Yin et al., Phys. Rev. Lett., **100**, 066406 (2008)

[91] H. Jiang et al., Phys. Rev. B, **82**, 045108 (2010)

[92] L. Sangaletti et al., Solid State Commun., **103**, 421 (1997)

[93] L. Soriano et al., Phys. Rev. B, **75**, 233417 (2007)

[94] I. Preda et al., Phys. Rev. B, **77**, 075411 (2008)

[95] R.J.O. Mossanek et al., Chem. Phys. Lett., **501**, 437 (2011)

[96] T. Haupricht, J. Weinen, A. Tanaka, R. Gierth, S.G. Altendorf, Y.-Y. Chin, T. Willers, J. Gegner, H. Fujiwara, F. Strigari, A. Hendricks, D. Regesch, Z. Hu, Hua Wu, K.-D. Tsuei, Y.F. Liao, H.H. Hsieh, H.-J. Lin, C.T. Chen, and L.H. Tjeng (unpublished)

[97] S.L. Molodtsov et al., Phys. Rev. Lett., **85**, 4184 (2000)

[98] C.J. Powell and A. Jablonski, Surf. Interface Anal., **29**, 108 (2000)

[99] S. Altieri et al., Phys. Rev. B, **61**, 13403 (2000)

[100] D. Alders et al., Phys. Rev. B, **57**, 11623 (1998)

[101] M.W. Haverkort et al., Phys. Rev. B, **69**, 020408 (2004)

[102] Parameters used for the calculation of the NiO_6 cluster (in eV): Δ=5.0, U_{dd}=6.5, $10Dq$=0.5, T_{pp}=0.8, $V(e_g)$=2.2, $V(t_{2g})$=$V(e_g)/2$, ζ see Ref. 22, Slater integrals 70% of Hartree-Fock values

[103] M.A. van Veenendaal and G.A. Sawatzky, Phys. Rev. Lett., **70**, 2459 (1993)

[104] M. Taguchi et al., Phys. Rev. Lett., **100**, 206401 (2008)

[105] A. Tanaka, J. Phys. Soc. Jpn., **68**, 3493 (1999)